Supplement of Earth Syst. Dynam., 12, 819–835, 2021
https://doi.org/10.5194/esd-12-819-2021-supplement

Supplement of

Abrupt climate change as a rate-dependent cascading tipping point

Johannes Lohmann et al.

Correspondence to: Johannes Lohmann (johannes.lohmann@nbi.ku.dk)

S1. FOLD BIFURCATIONS IN THE SEA ICE COMPONENT

The sea ice component of our coupled model shows a fold-fold bifurcation structure, which usually manifests itself in a characteristic 'S-shaped' bifurcation diagram. However, when choosing low values of h in the model, the bifurcation diagram is rather 'Z-shaped' instead. This is due to the steeper transition in the hyperbolic tangent of the underlying ODE (Eq. 5 in the main text), which corresponds to a steeper albedo transition from open ocean to full ice cover. The value of h is largely a modeling choice, which depends on what region of the ocean our box should represent. In this work, our choice $h = 0.5$ differs from the value $h = 0.08$ used by Eisenman et al. (2012)[3]. This yields an S-shaped instead of a Z-shaped bifurcation diagram. The effect of this change in h on the albedo transition and resulting bifurcation diagrams is illustrated in Fig. S1. Since we are modeling a large ocean basin, we considered it more appropriate to use a more gradual albedo transition, corresponding to a wider range of partial sea ice cover. The choice of h does not change our results, however, besides the fact that for lower values of h it would be more difficult to detect a critical slowing down in the sea ice variable. This is because for such a 'Z-shaped' fold-fold bifurcation structure, the curvature of the underlying potential around the equilibria only changes significantly when relatively close to a bifurcation point.

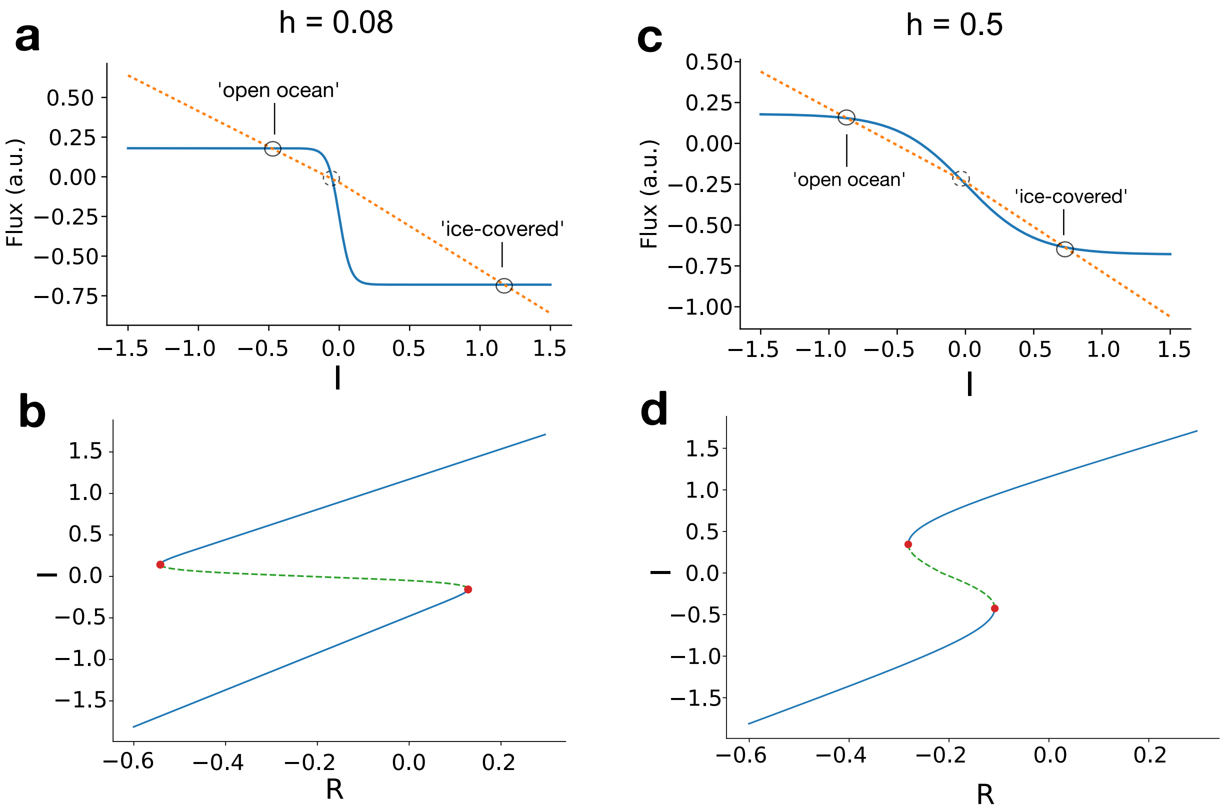

FIG. S1. Equilibria of the sea ice component. Panels **a** and **c** show different terms of the right hand side of the ODE that defines the model (Eq. 5 in the main text). $R = 0.0$ and $R = -0.2$ is used in **a** and **c**, respectively. The blue solid curve comprises the incoming shortwave and longwave radiation, i.e. is equal to $-\Delta \tanh\left(\frac{I}{h}\right) - L + 1$. The orange dotted curve comprises the remaining, piecewise-linear terms, i.e. the outgoing radiation, the export and import of sea ice, as well as the ocean heat flux. The intersections of the curves gives the equilibria, where $dI/dt = 0$. Shown are two different values of the parameter h, which determines how gradual the albedo transition from open ocean to full ice cover is. Bifurcation diagrams with R as control parameter are given in **b** and **d**, where the unstable equilibrium is indicated by the dashed line.

S2. BIFURCATION DIAGRAM OF THE COUPLED MODEL

The model presented in the paper is unidirectionally and linearly coupled. For our purposes, it was easiest and sufficient to understand the model dynamics in terms of the individual bifurcation diagrams for I with R as control parameter, and for T with $\eta_1(I)$ as control parameter, as presented in the main text. Nevertheless, Fig. S2 shows bifurcation diagrams of the coupled model with R as control parameter. A unidirectional coupling of two systems with a fold-fold bifurcation leads to a 'quadruple' fold (see e.g. Dekker et al. 2018[1]), due to the combinations of all different stable and unstable branches of equilibria of the two sub-systems. Additionally to the situation discussed in the paper, where (depending on the rate of the parameter shift) the system tips from a state with collapsed circulation and full sea ice cover to either a state with vigorous circulation and no sea ice cover, or to a state with (still) collapsed circulation and no sea ice cover, there exists also a stable state with vigorous circulation and full sea ice cover, as well as a variety of unstable equilibria. All stable and unstable equilibria are labeled accordingly in Fig. S2c. The figure also includes two trajectories with different rates of the parameter shift, which correspond to the cascade presented in the main text, with the exception of a different value of h.

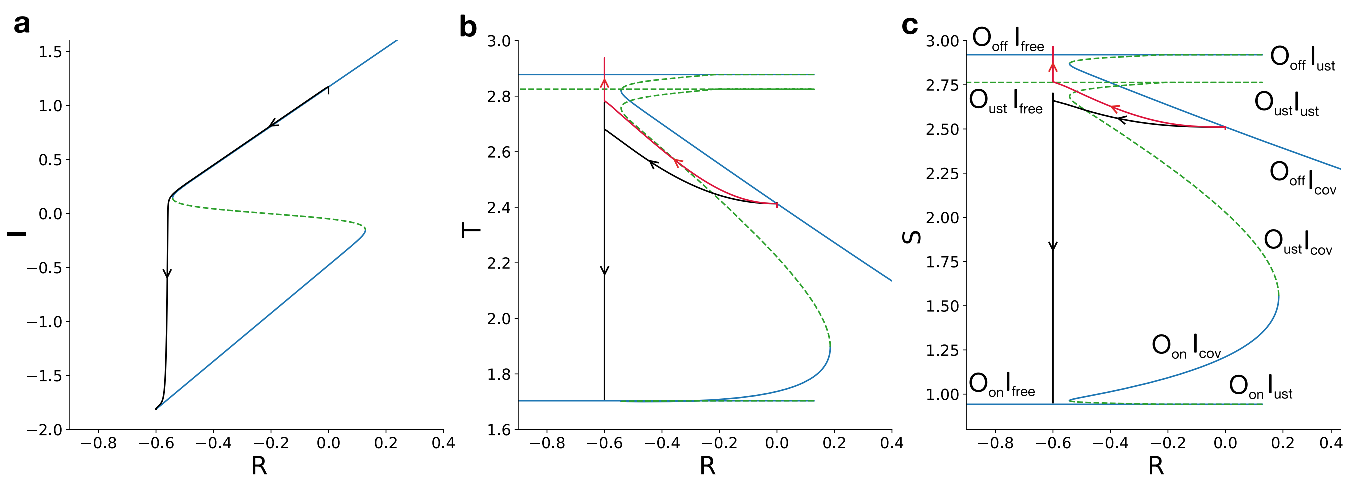

FIG. S2. Bifurcation diagrams of the deterministic coupled model with $h = 0.08$ (Eq. 6 in the main text) for the individual variables I (**a**), T (**b**) and S (**c**) with R as control parameter. Solid blue (dashed green) lines indicate stable (unstable) equilibria. In panel **c** the individual branches of equilibria are labeled, according to the ocean state 'O' and the sea ice state 'I'. The ocean circulation can be in a vigorous (O_{on}), or collapsed state (O_{off}), and the sea ice state can be ice free (I_{free}) or ice-covered (I_{cov}). Further, there are a variety of unstable states, where either the (isolated) sea ice or ocean components assume an unstable equilibrium (I_{ust} and O_{ust}). Also shown are two trajectories, where R is ramped linearly from 0 to -0.6 at rates below (red) and above (black) the critical rate.

S3. NON-SMOOTH FOLD IN THE STOMMEL MODEL

The Stommel model is a non-smooth dynamical system due to the use of an absolute value in its equations. Thus, there is a boundary in phase space, given by the line $T = S$, which separates two regimes of the flow. This can be seen by the discontinuity in the real part of the eigenvalue λ_1 of the Jacobian, shown in Fig. S3. Additionally, one of the fold bifurcations when varying η_1 occurs due to a collision of the saddle and the 'off' stable equilibrium on this boundary. Such a bifurcation is called a non-smooth fold (see e.g. di Bernardo et al., 2008[2]). In Fig. S3, this bifurcation is shown by the red solid line ('off' equilibrium) and the black dashed line (saddle), which meet in a cusp. As a result, the 'off' equilibrium already comes very close to the basin boundary significantly prior to the bifurcation point. In contrast, for the smooth fold bifurcation of the 'on' equilibrium (collision of the solid and dashed black lines) this is not the case. This is the origin of the 'soft' tipping behaviour discussed in the main article, and shown in Fig. 7 specifically.

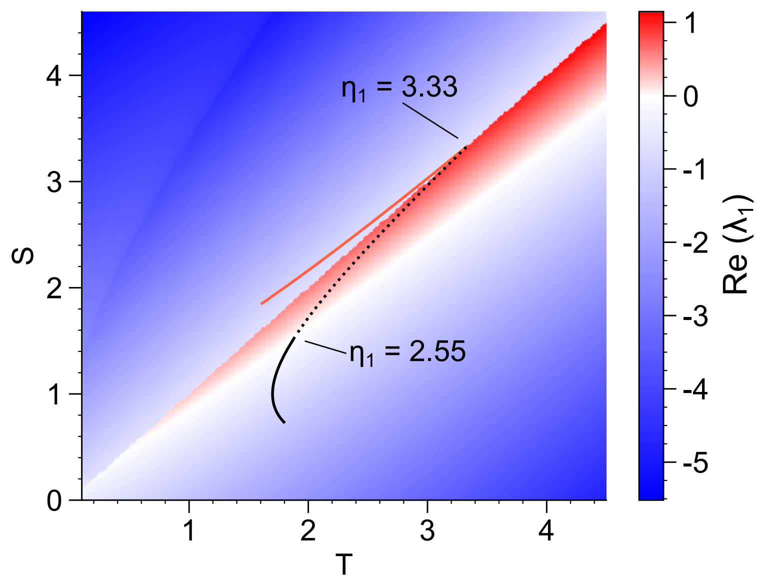

FIG. S3. Real part of the first eigenvalue λ_1 of the Jacobian of the Stommel model with $\eta_3 = 0.3$ (color map). Note that since η_1 and η_2 are additive parameters, they don't influence the Jacobian. Also shown are the curves of equilibria in the model when changing η_1 with fixed $\eta_2 = 1.0$. The red curve are the stable 'off' equilibria for $\eta_1 = 2.0$ to $\eta_1 = 3.33$, the solid black curve are the stable 'on' equilibria for $\eta_1 = 2.55$ to $\eta_1 = 3.7$, and the dashed black curve shows the saddle equilibria for $\eta_1 = 2.55$ to $\eta_1 = 3.33$.

S4. ESTIMATION OF EARLY-WARNING SIGNALS FROM TIME SERIES

From the trend in a time series it is hard to infer whether an abrupt transition is imminent, and what type of transition this might be. Instead, most early-warning signals aim to extract generic features in the fluctuations around a trend that occur as a tipping point is approached. We consider several early-warning indicators leading up to the tipping points by estimating statistical properties of the fluctuations in a sliding window. The trends encountered here are due to the system dynamics trying to catch up with the moving equilibria during a parameter shift, and are nonlinear. Thus, to separate the fluctuations from the trend, a nonlinear detrending is necessary. We do this by subtracting a fit with a cubic function to the time series in the sliding window. While higher-order polynomials could more accurately detrend the signal, they would also remove more of the variability around the trend. As a result, the only free parameter is the sliding window size.

Choosing the optimal window size is done by two trade-offs. First, a significant early-warning signal needs to be achieved. Here, there is a trade-off between low uncertainty of the estimator (large window) and sufficient temporal resolution to detect the changes in the fluctuations before the transition (small window). The required temporal resolution depends on how fast the tipping point is approached. If it is approached fast, there is only a short time frame during which changes in the fluctuations occur. Second, there is a trade-off between removing the non-linear trend as precisely as possible (small window) and preserving as much of the variability used to detect the early-warning signal as possible (large window). If the window is chosen too large, there remains a residual trend, which leads to artifacts in the statistical indicators, depending on the noise level. This effect is shown in Fig. S4. Considering these trade-offs, we use a window size of 150 years for the simulations with the coupled model, and 200 years for simulations with the Stommel model. In the latter case there is a slightly smoother trend since no rapid transition of the sea ice is involved. The results are not sensitive to the precise values.

We note that the choice of the detrending method and sliding window size should also depend on the noise level and the rate of the parameter shift. However, for our purposes these two factors are tightly constrained. The rate of the parameter shift is chosen fast enough to obtain a dynamical regime with rate-induced transitions, but slow enough so that it is possible to consider early-warning indicators. The noise levels are constrained because we aim for a regime where there is significant tipping variability and delays, but not too many noise-induced transitions (see Sec. IIIB).

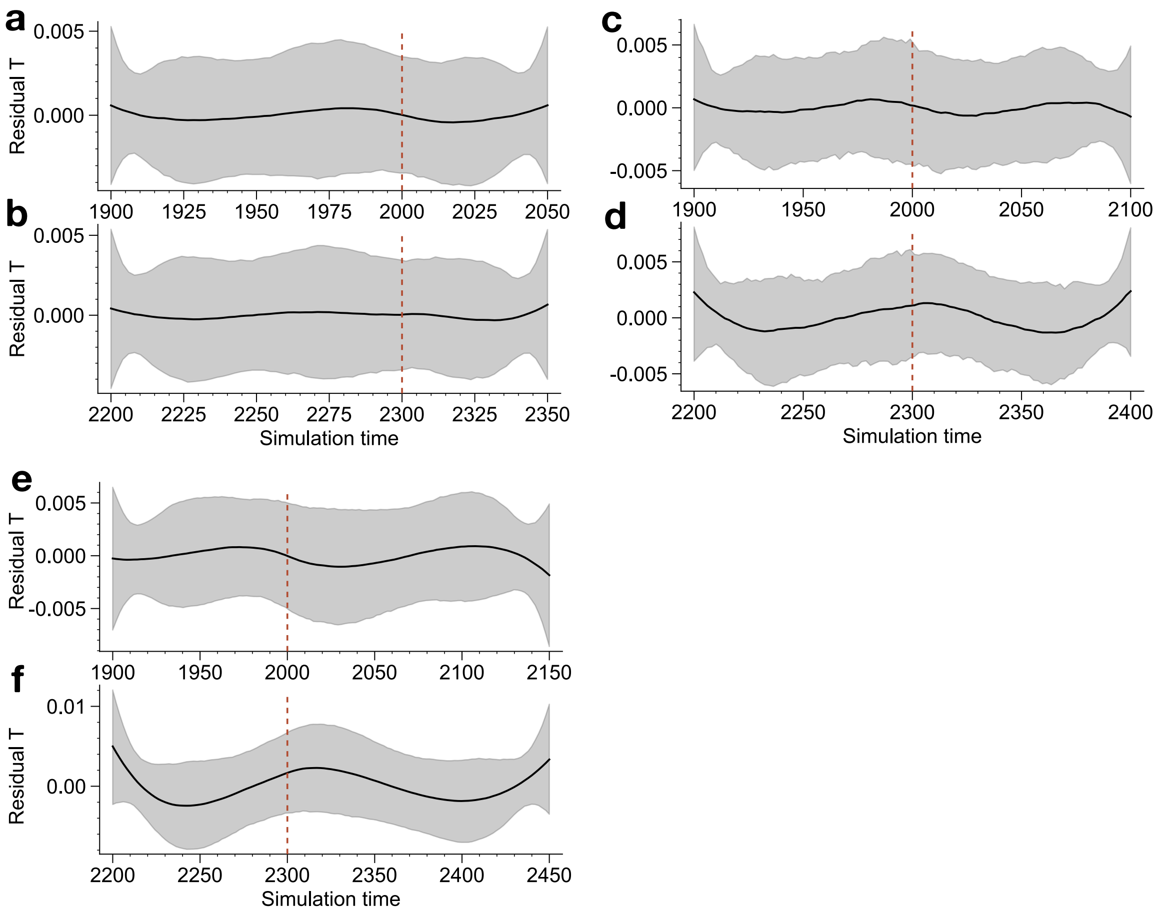

FIG. S4. Residuals after detrending with a cubic function of simulations with the Stommel model ($\sigma_T = \sigma_S = 0.2$), where η_1 is ramped from $\eta_1 = 2.65$ to $\eta_1 = 3.00$ within 300 years. The mean residuals are shown as the black line, and the gray shading illustrates the region in between the 5- and 95-percentile. The detrending is shown for a window of 150 years (**a-b**), 200 years (**c-d**), and 250 years (**e-f**). Panels **a**, **c** and **e** show time windows around the start of the parameter shift (red dashed line), whereas panels **b**, **d** and **f** show time windows around the end of the parameter shift (red dashed line). In **e** and **f** the average residuals show the remaining trends due to the imperfect fit of a cubic function to the non-linear trend of the model variables, which are as large as the residual fluctuations (shading). Thus, the window is chosen too wide in this case.

S5. JACOBIAN ESTIMATED FROM TIME SERIES IN THE STOMMEL MODEL

In this paper we propose an early warning signal for rate-induced tipping based on estimating the Jacobian from noisy time series. In Fig. S5 we show that using the method presented in the Appendix A, the Jacobian in the vicinity of the fixed points as well as the saddle of the Stommel model can be inferred correctly with only a small quantitative bias. From simulations where the parameter η_1 is shifted from $\eta_1 = 2.65$ to $\eta_1 = 3.0$ within 300 years, we extract the part of the time series where the system is in the vicinity of the saddle (see Fig. 13), and detrend with a cubic function. Here only realizations are chosen where the systems stays in the vicinity of the saddle for at least 1000 years. For each realization, we also choose segments of the same length before and after the parameter shift to estimate the Jacobian around the 'off' attractor at $\eta_1 = 2.65$ (black) and the 'on' attractor at $\eta_1 = 3.0$, respectively. This gives rise to the three distributions of each Jacobian element around the saddle (orange), 'off' attractor (black), and 'on' attractor (blue) in each panel of the figure.

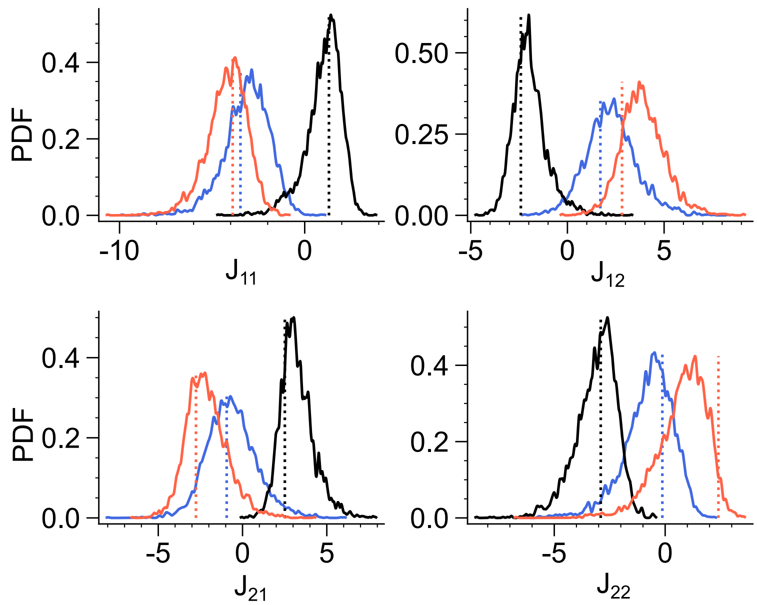

FIG. S5. Distributions of estimates of the Jacobian elements in the Stommel model ($\sigma_T = \sigma_S = 0.2$) from an ensemble of simulations where η_1 is ramped from $\eta_1 = 2.65$ to $\eta_1 = 3.0$ within 300 years. The different distributions represent the Jacobian elements around the 'off' attractor at $\eta_1 = 2.65$ (black), the 'on' attractor at $\eta_1 = 3.0$ (blue) and the saddle (red, see main text for more information). Only realizations have been chosen where the system spent at least 1000 years close to the saddle. The dashed lines correspond to the true values at the corresponding fixed points.

* johannes.lohmann@nbi.ku.dk

[1] Dekker, M. M., von der Heydt, A. S., and Dijkstra, H. A.: Cascading transitions in the climate system, Earth Syst. Dynam., 9, 1243–1260, 2018.

[2] di Bernardo, M., Budd, C. J., Champneys, A. R., Kowalczyk, P., Nordmark, A. B., Tost, G. O., and Piiroinen, P. T.: Bifurcations in Nonsmooth Dynamical Systems, SIAM Review, 50, 629–701, 2008.

[3] Eisenman, I.: Factors controlling the bifurcation structure of sea ice retreat, J. Geophys. Res., 117, D01 111, 2012.